Defence Technology xxx (xxxx) xxx

Contents lists available at ScienceDirect

Defence Technology

journal homepage: www.elsevier.com/locate/dt

Optimizing the defensive characteristics of mild steel via the electrodeposition of Zn–Si_3N_4 reinforcing particles

I.G. Akande [a, *], O.O. Oluwole [a], O.S.I. Fayomi [b, c]

[a] Department of Mechanical Engineering, University of Ibadan, Ibadan, Oyo state, Nigeria
[b] Department of Mechanical Engineering, Covenant University, ota, ogun state, Nigeria
[c] Department of Chemical, Metallurgical and Materials Engineering, Tshwane University of Technology, Pretoria, South Africa

ARTICLE INFO

Article history:
Received 2 September 2018
Received in revised form
30 October 2018
Accepted 2 November 2018
Available online xxx

Keywords:
Polarization
Corrosion
Microhardness
Coating
Composite
Matrix

ABSTRACT

The effect of Zn–Si_3N_4 deposition prepared via direct electrolytic co-deposition on mild steel was studied as a result its inherent vulnerability to corrosion in an aggressive environment and failure on the application of load. The experiment was conducted varying the mass concentration of silicon nitride (Si_3N_4) between 7 and 13 g at cell voltage of 0.3 and 0.5 V, at constant temperature of 45 °C. The morphologies of the coated surfaces were characterized using high resolution Nikon Optical Microscope and Scanning Electron Microscope (SEM) revealing that the particles of the Zn–Si_3N_4 were homogeneously dispersed. The corrosion behaviour was studied using potentiodynamic polarization technique in 3.65% NaCl solution and the microhardness was examined using Brinell hardness testing technique. The result of the corrosion experiment confirmed an improved corrosion resistance with a reduction in corrosion rate from 9.7425 mm/year to 0.10847 mm/year, maximum coating efficiency of 98.9%, maximum polarization resistance of 1555.3 Ω and a very low current density of 9.33×10^{-6} A/cm^2. The negative shift in the E_{corr} revealed the cathodic protective nature of the coating. The microhardness was also found to have increased from 137.9 HBN for the unmodified steel to a maximum value of 263.3 HBN for the 0.5Zn–13Si_3N_4 coated steel representing 90.9% increment in hardness as a result of the matrix grain refining and dispersion-strengthening ability of the incorporated Si_3N_4 particles.

1. Introduction

In recent time, incessant failure of engineering materials have orchestrated the application of coating technology as a reliable defence mechanism in automotive, manufacturing, aerospace and chemical processing industries [1]. Composite coating is of a rare quality, enabling the deposition of insoluble nano-particles of ceramic, metallic and non metallic alloys into electrolytic bath for specified chemical, mechanical and functional properties [2–8]. Metal matrix reinforced with nano particles generally exhibit wide range of engineering applications due to improved hardness and ability to withstand corrosion and wear [9–14]. Zn incorporated nano composite coatings have been confirmed to posses' good surface properties which is not unconnected to the strengthening effect of the embedded particles [15]. However, these properties can be made better through the incorporation of Si_3N_4 nano particles [16]. By virtue of the strength, hardness, good fracture toughness and thermal resistance, silicon nitride based ceramic have been a good choice for structural component application such as ball bearings and cutting tool applications [17–19]. Although attempted codeposition of hard particles such as Al_2O_3, TiO_2, SiC, WC, Cr_3C_2, TiC and diamond on steel had been done focusing more on the improvement of wear resistance [20]. In view of this, Zn nanocomposite coating reinforced with Si_3N_4 particles was developed with some incorporated desired properties. Si_3N_4, being a versatile ceramic was chosen because of its impeccable performance when high strength, high hardness as well as good resistance to thermal shock is required [21–23]. The excellent mechanical properties [24,25] of Silicon nitride ceramic are the reasons for the attraction in numbers of application such as engine components, spacecrafts and high-temperature electronics [26–28].

* Corresponding author.
E-mail address: aigodwin2015@gmail.com (I.G. Akande).
Peer review under responsibility of China Ordnance Society

https://doi.org/10.1016/j.dt.2018.11.001

2. Experimental procedure

2.1. Preparation of substrates

Mild steel of dimension (50 mm × 30 mm x 2 mm) whose chemical composition is shown in Table 1 was used as the cathode substrate and 99.9% zinc plate of (60 mm × 40 mm x 10 mm) were prepared as anodes. The surface of the steel was well polished with emery papers of different grades as recommend in the previously by authors Ref. [29,30]. The samples were surface cleaned by immersion in 0.01 M of sodium carbonate solution at ambient temperature of 25 °C for 10 s. They were pickled and activated with 10% hydrochloric acid at ambient temperature for 10 s, followed by quick rinsing in deionized water.

2.2. Deposition of Zn–Si_3N_4

The bath prepared for the coating process using the parameters in Table 2 was subjected to continuous stirring at 300 rpm and 45 °C constant heating throughout the coating process in order to obtain stability in suspension, avoiding particles' agglomeration. Prevention of agglomeration of particles enhances the mobility electrophoresis of the solution [31]. The agitations of bath do not only keep the Zn–Si_3N_4 particles suspended in the electrolyte but also assist their mass transportation to the cathode surface. Investigations of various researchers have shown that increased agitation generally enhances the amount of particles in the metal deposit. However, too much or immoderate agitation may influence the movement of the electrodes, alter the charge transfer region and more so, result to a lower quantity of particles in the metal deposit [32]. In the plating process, the prepared mild steel being the cathode was positioned in between two zinc plates and connected to the negative terminal of the rectifier in the electrodeposition bath. The zinc (anode) were also immersed and connected to the positive terminal of the rectifier [33,34]. The gap between the cathode and anodes was 3 cm. The cathode was positioned equidistance from the anodes. The pH, deposition time, current density and temperature were kept constant as shown in Table 2 varying the mass concentration of Si_3N_4 and cell voltage. The following reactions occurred between zinc and the base metal during the electrodeposition process

$$\text{At the anode, } Zn \rightarrow Zn^{2+} + 2e^{-} \text{ (Oxidation reaction)} \quad (1)$$

$$\text{At the cathode, } Fe^{2+} + 2e^{-} \rightarrow Fe \text{ (Reduction reaction)} \quad (2)$$

$$\text{Overall Cell reaction, } Zn + Fe^{2+} \rightarrow Zn^{2+} + Fe \quad (3)$$

2.3. Characterization of samples and structural test

The surface adhesion and homogeneous dispersion of Zn– Si_3N_4 on the mild steel resulted in the development of remarkable structures. This was examined using high resolution Nikon Optical Microscope and Scanning Electron Microscope (SEM). The images were taken at 100× and 500× magnifications respectively. Potentiodynamic polarization assessment and Brinell technique at a load of 30 g for a period of 20 s were used to characterize corrosion and hardness of the coated and uncoated steels. Measurements of the coating thickness were carried out using Elcometer microthickness meter guage (Elcometer 456 Model) with the accuracy of ±1%. The thickness of all the samples were measured at different points and the thickness average were obtained for each of the samples and recorded as shown in Table 3.

Table 2
Process parameter for Zn–Si_3N_4 sulphate bath formulation.

Composition	Mass concentration
K_2SO_4	50 g/L
$ZnSO_4$	130 g/L
$NaSO_4$	30 g/L
Thiourea	10 g/L
NaCl	35 g/L
Boric acid	10 g/L
Glycine	10 g/L
Si_3N_4	7/13 g/L
pH	4.5
Current density	2 A/cm^2
Cell Voltage	0.3/0.5 V
Time	15 min
Temp.	45 ^{O}C

2.4. Electrochemical test

A three-electrode cell assembled in a 3.65% NaCl static solution with Autolab PGSTAT 101 Metrohm Potentiostat connected to NOVA 2.1.2 soft ware via computer system was used to examine the anti-corrosion behaviour of the composite coatings at ambient temperature of 25 °C. The steel acted as the working electrode, platinum electrode as the counter electrode and Ag/AgCl was made the reference electrode. Potentiodynamic polarization curves were obtained from cathodic potential of −1.5 V to anodic potential of 1.5 V versus open circuit potential at a sweep rate (scan rate) of 0.005 m/s. This was carried out in similitude to our recent research work [35].

2.5. Mechanism of zinc corrosion in 3.65% NaCl solution

Many researchers have reported zinc hydroxide chloride as corrosion products of zinc in NaCl solution [36–38]. Obviously, zinc hydroxide chloride is one of the corrosion layer compounds formed after immersion in 3.65% NaCl solution. A lot of studies on corrosion behaviour of zinc in NaCl solutions have shown that corrosion of zinc precedes two partial reactions [39,40]. The cathodic reaction in Eq. (4) corresponds to the reduction of oxygen which could leads to a local increase in pH value in the depth of corrosion damages and consequently resulting to the formation of zinc hydroxide chloride in the pits and their neighbourhood areas [41]. The anodic reaction involves the dissolution of zinc as shown by Eq. (5). Expectedly, zinc cation and the hydroxide anion react to form zinc hydroxide presented by Eq. (6). At the active cathodic site, zincate ions is produced as indicated by Eq. (7) provided the pH is large enough. In the presence of Sodium Chloride, Chloride ions (Cl^{-}) migrate to the anodic site where Zinc hydroxide chloride is formed as shown in Eq. (8)

Table 1
Chemical composition of the mild steel used.

Element	C	Mn	Si	P	Cu	S	Ni	Cr	Fe
Wt %	0.210	0.468	0.156	0.026	0.007	0.023	0.004	0.021	Balance

Please cite this article as: Akande IG et al., Optimizing the defensive characteristics of mild steel via the electrodeposition of Zn–Si_3N_4 reinforcing particles, Defence Technology, https://doi.org/10.1016/j.dt.2018.11.001

Table 3
Itinerary parameters of Zn− Si_3N_4 alloy co-deposition.

Samples	Time/min	Coating thickness/μm	Weight gained/g	Coating per unit area/(mg·mm^{-2})
Control	–	–	–	–
0.3Zn− 7Si_3N_4	15	138.2	0.11	0.073333
0.5 Zn− 7Si_3N_4	15	169.3	0.43	0.286667
0.3 Zn− 13Si_3N_4	15	166.1	0.37	0.246667
0.5Zn− 13Si_3N_4	15	175 .7	0.48	0.320000

$$O_{2\ (d)} + 2H_2O + 4e^- \rightarrow 4OH^-_{(aq)}\ \text{[Cathode]} \quad (4)$$

$$Zn \rightarrow Zn^{2+} + 2e^-\ \text{[Anode]} \quad (5)$$

$$Zn^{2+} + 2OH^- \rightarrow Zn(OH)_2 \quad (6)$$

$$Zn(OH)_{2+}\ 2OH^- \rightarrow Zn(OH)_4^{2-} \quad (7)$$

$$5Zn(OH)_2 + 2Cl^- + H_2O \rightarrow Zn_5(OH)_8\ Cl.H_2O + 2OH^- \quad (8)$$

3. Results and discussion

3.1. Structural analysis of uncoated and Zn− Si_3N_4 deposited mild steel

The Optical micrographs of the uncoated mild steel, Zn− Si_3N_4 coated at 7 %w and 13 %w are shown in Figs. 1–3 respectively. From the structural characterization, as expected, the uncoated mild steel surface as shown in Fig. 1 looked rough exhibits the inherent pitting corrosion initiation tendency [42,43]. On the other hand, several crystal growths was seen to have developed on the interface of the coated mild steels in Figs. 2 and 3 exhibiting a defect free surface. With the 7 %w in Fig. 2(a) and b, though Fig. 2(a) appears smoother but visible flake-like crystalline pattern were seen at the general interface, which are more obvious in Fig. 2(b). The unique microstructure displayed by the composite can be linked to the inclusion and homogeneous dispersion of Si_3N_4 nanoparticles in the Zn matrix, promoting the increase in number of nucleation site and impeding crystal growth, resulting in the generation of small nano-sized metal grains [15,44].

In the same vein, the 13 %w coated mild steel shown in Fig. 3(c) and d exhibit similar structures as the 7 %w coated but appeared relatively smoother. It is worthy of note that the 0.5Zn− 13Si_3N_4 coated steel has the smoothest structure compare to all other coated samples as revealed by the optical microscope. This might be attributed to the increase in mass concentration of Si_3N_4 nanoparticle, minimising the formation of flake-like crystalline pattern. It has been reported that, increasing mass concentration of particles increase the coating thickness leading to less coarse surfaces [45]. However, it is worth mentioning that the process parameters can influence the surface texture which may alter the performance and life span of the coating [44].

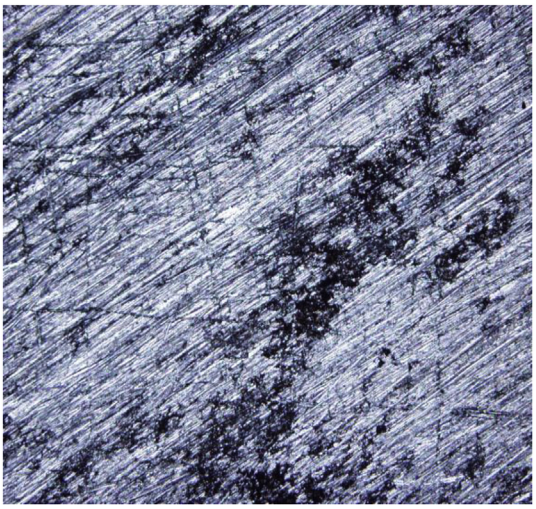

Fig. 1. Optical micrograph of uncoated mild steel

SEM micrographs Zn− Si_3N_4 coated mild steel at 7%w and 13%w are shown in Figs. 4 and 5 SEM images of the samples show that the pitting evolution at the interface was apparently invisible. Good surface topography, morphological and coverage were observed. The well dispersed quality of the coated surface hindered the ingression of the corrosive ion into the metallic interface. The surface of the sample shown in Figs. 4(b) and 5c appeared rougher, which is in unison with the images of Optical micrograph.

The SEM images, in accordance with the work of author Ref. [46] reveal that the zinc interface clearly displayed nodular structures on the coating network with redefined morphology making it look alluring. Expectedly, the path of nucleation started from the zinc metal as load carrier; the dissemination of the particulates involves the nucleation domains and therefore improving the formed nanocomposites. It is also worthy of note that the SEM micrographs reveal images with low porosity.

3.2. Electrochemical test result of Zn− Si_3N_4 coated and uncoated mild steel

Potentiodynamic polarization test performed on Zn− Si_3N_4 coated steel confirmed its ability to resist corrosion in 3.65% NaCl solution. The result of the corrosion experiment obtained from the extrapolation of Tafel curve shown in Fig. 6 confirmed an improved corrosion resistance with a reduction in corrosion rate from 9.7425 mm/year to 0.10847 mm/year as indicated in Table 4, maximum polarization resistance of 1555.3 Ω and a very low current density of 9.33×10^{-6} A/cm^2. This shows that the coating blocked the active sites of the modified steel impeding the exchange of current. The coatings were able to act as barrier, therefore minimising the cathodic evolution and anodic metal dissolution reactions of the mild steel [47,48]. The presence of Si_3N_4 nanoparticles decreases the concentration of chloride ion, resulting in a lower current density in the charge transfer controlled and mixed potential region. At the mixed potential region, the value of corrosion potential depends on the rate of both the cathodic as well as anodic reaction. The rate of the charge transfer reaction at the interface depends not only on the applied potential but also on the concentration of reacting species prevailing at the electrode surface [49].

From the results obtained, all the corrosion parameters favoured 0.5Zn−13Si_3N_4 coated sample. This may be as a result of the increased concentration of Si_3N_4 leading to the reduction of the adsorption of chloride ion in aggressive environment [50,51]. It can

Please cite this article as: Akande IG et al., Optimizing the defensive characteristics of mild steel via the electrodeposition of Zn−Si_3N_4 reinforcing particles, Defence Technology, https://doi.org/10.1016/j.dt.2018.11.001

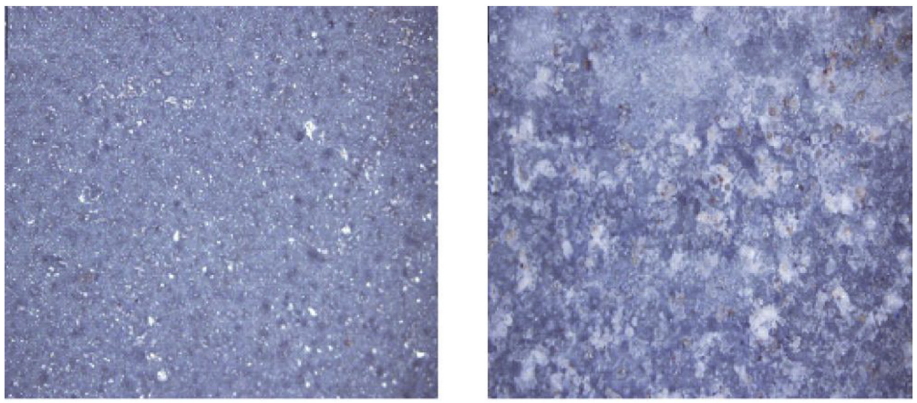

(a) 0.3Zn-7Si_3N_4 (b) 0.5Zn-7Si_3N_4

Fig. 2. Optical micrographs of (a) 0.3 Zn−7Si_3N_4 coated mild steel and (b) 0.5 Zn−7Si_3N_4 coated mild steel.

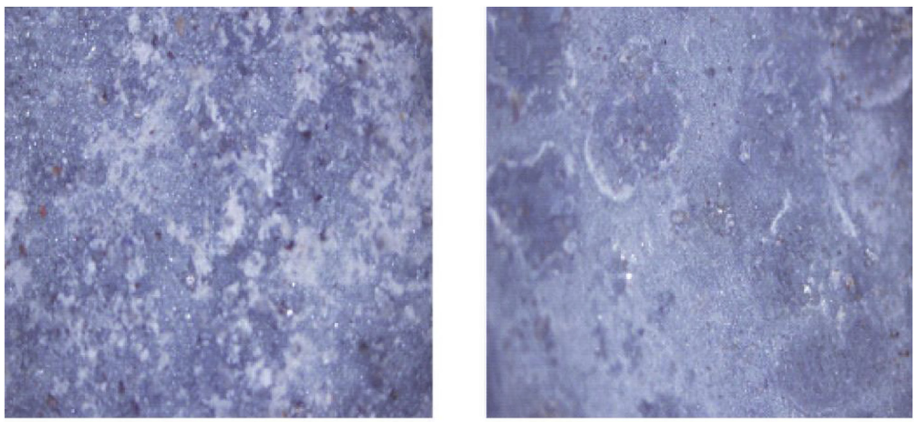

(a) 0.3Zn-13Si_3N_4 (b) 0.5Zn-13Si_3N_4

Fig. 3. Optical micrographs of (c) 0.3 Zn−13Si_3N_4 coated mild steel and (d) 0.5Zn−13Si_3N_4 coated mild steel.

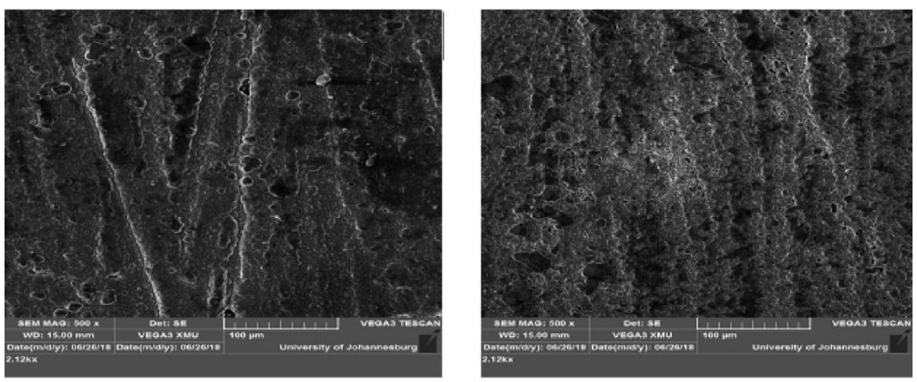

(a) 0.3Zn-7Si_3N_4 (b) 0.5Zn-7Si_3N_4

Fig. 4. SEM micrographs of (a) 0.3 Zn−7Si_3N_4 coated mild steel and (b) 0.5Zn−7Si_3N_4 coated mild steel.

also be traced to the nature and adhesiveness of the passive film produced by 0.5Zn−13Si_3N_4 on the surface of the coated steel or chemical stability of the samples [52]. The negative shift in the E_{corr} confirms the cathodic protective nature of the coating [53,54]. Generally, Zn− Si_3N_4 was found to have reduced the current density of all the coated samples. The reduction in current densities could be attributed to blockage of the active sites of the steel by the Zn−Si_3N_4 particles.

Fig. 7 shows the OCP versus time curves for the uncoated and Zn−Si_3N_4 coated steel in 3.65% NaCl static solution. Carefully examining the OCP vs. time curves, it can be seen that the presences Zn−Si_3N_4 shifted the potential of the steady-state to more negative values. The notable shift is attributed to the predominant cathodic effect of Si_3N_4 on the mild steel indicating the cathodic reaction is

Please cite this article as: Akande IG et al., Optimizing the defensive characteristics of mild steel via the electrodeposition of Zn−Si_3N_4 reinforcing particles, Defence Technology, https://doi.org/10.1016/j.dt.2018.11.001

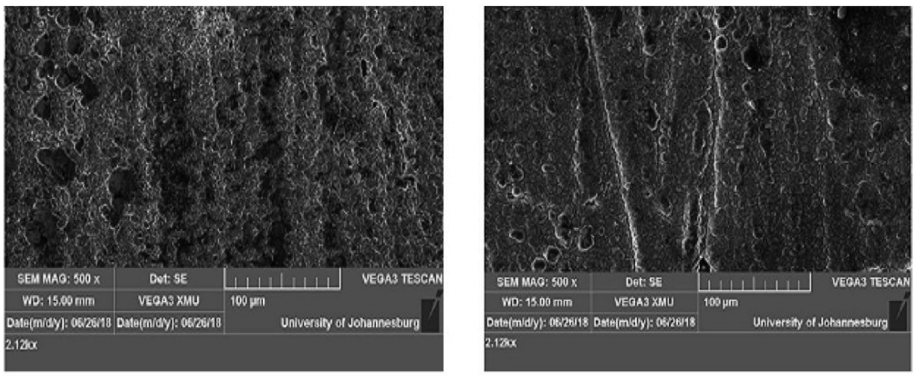

(a) 0.3Zn-13Si_3N_4 (b) 0.5Zn-13Si_3N_4

Fig. 5. SEM micrographs (c) 0.3 Zn− 13Si_3N_4 coated mild steel and (d) 0.5Zn− 13Si_3N_4 coated mild steel.

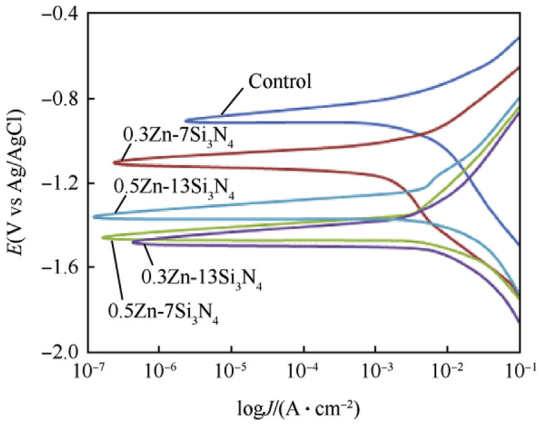

Fig. 6. Potentiodynamic Polarization curves for uncoated and Zn−Si_3N_4 Composite coated mild steel in 3.65% NaCl medium.

Table 4
Potentiodynamic Polarization parameters for uncoated and Zn− Si_3N_4 Composite coated mild steel in 3.65% NaCl medium.

Samples	E_{corr}/V	j_{corr}/(A·cm^{-2})	CR/year	PR/Ω
Control	−0.906982	8.38E-04	9.74250	95.580
0.3Zn−7Si_3N_4	−1.106870	2.35E-05	0.27307	184.360
0.5Zn−7Si_3N_4	−1.460570	1.61E-05	0.18703	432.890
0.3Zn−13Si_3N_4	−1.481630	4.28E-05	0.49728	992.892
0.5Zn−13Si_3N_4	−1.362300	9.33E-06	0.10847	1555.300

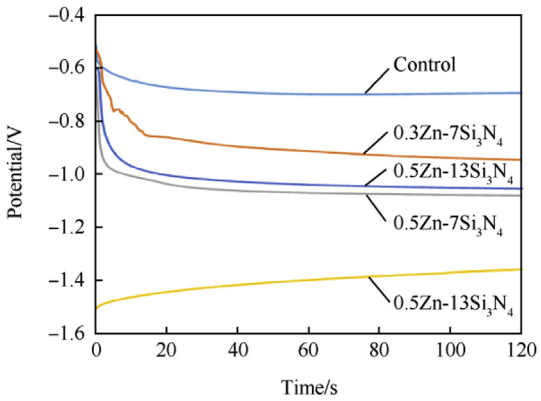

Fig. 7. Evolution of open circuit potential (OCP) vs. exposure time for the uncoated and Zn− Si_3N_4 Composite coated mild steel in 3.65% NaCl medium.

relatively more affected than the anodic reaction [1,51]. It is important to note that the OCP vs. time curve for the coated and uncoated samples were near straight line indicating that steady state potential was attained [54].

3.3. Coating efficiency

The percentage coating efficiency (% *CE*) was calculated using equation (9) [55–59].

$$C.E\% = 1 - \frac{j_{corr}}{j_{ocorr}} X\ 100 \quad (9)$$

j_{corr}, the corrosion current densities for the coated samples and j_{ocorr}, corrosion current density for the uncoated sample. It can be seen in Fig. 8 that 0.5Zn−13Si_3N_4 coated steel exhibits the highest coating efficiency of 98.9%. This might be due to the higher concentration of Si_3N_4 and the value of cell voltage, thereby influencing the increase in deposition of the particles leading to higher value of thickness, 175.7 µm and effective covering of the steel, preventing the ingression of chloride ion [45,51]. Generally the coating efficiency of Zn−Si_3N_4 was found to be on a high side with the minimum value of 94.9%.

3.4. Microhardness analysis of Zn−Si_3N_4 coated and uncoated samples

The microhardness results obtained for the Zn−Si_3N_4 coated and uncoated steel were displayed in the chart in Fig. 9. These values were gotten using the Brinell hardness test technique. This is in accordance to ASTM A-370 [60]. Upon comparison, 0.5Zn−15-Si_3N_4 has the highest hardness value of 263.3 BHN. This represents 90.9% increment in the hardness compared to the unmodified mild

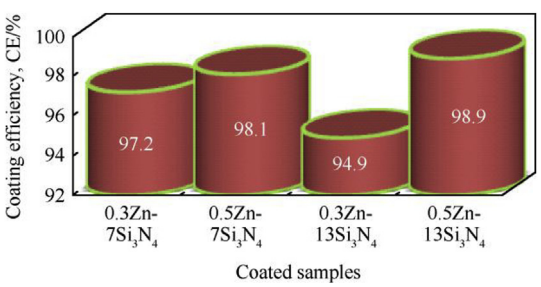

Fig. 8. Coating efficiency of Zn−Si_3N_4.

Please cite this article as: Akande IG et al., Optimizing the defensive characteristics of mild steel via the electrodeposition of Zn−Si_3N_4 reinforcing particles, Defence Technology, https://doi.org/10.1016/j.dt.2018.11.001

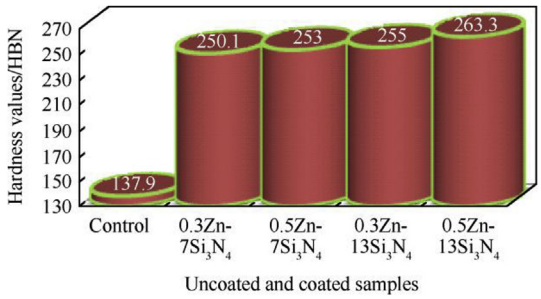

Fig. 9. Brinell hardness value for Zn− Si_3N_4 coated and uncoated samples.

steel.

In general, the hardness value for all the coated samples with varying additives showed an increase. The improvement in microhardness could be attributed to the formation of adhesive mechanism of the composite coating on the substrate sample, strain energy in the periphery of the composited coated steel by the particles in the matrix and operating factors such as bath constituents and other processing parameters [61–63].

4. Conclusions

(1) Zn−Si_3N_4 nanocomposite coatings have been successfully produced.
(2) The modified mild steel displayed strong strengthening behaviour with maximum hardness value of 263.3 HBN which amounts to 90.9% increment in hardness compared to the unmodified steel
(3) 0.5Zn−13Si_3N_4 proved to be the optimum bath loading for improved corrosion resistance, hardness and better surface structure.
(4) The result of the corrosion experiment on 0.5Zn−13Si_3N_4 coated mild steel confirmed an improved corrosion resistance with a reduction in corrosion rate from 9.7425 mm/year to 0.10847 mm/year, coating efficiency of 98.9%, polarization resistance of 1555.3 Ω and a very low current density of 9.33×10^6 A/cm^2.
(5) The negative shift in the E_{corr} reveals the predominant cathodic protective nature of the coating.

Acknowledgments

This is to acknowledge Department of Mechanical Engineering, University of Ibadan for the P.hD opportunity. Prof. Fayomi Ojo Isaac Sunday of Surface Engineering Research Centre, Covenant University Ota, Nigeria is deeply appreciated for the provision of laboratory facilities and technical advice.

References

[1] Kasturibai S, Kalaignan GP. Pulse electrodeposition and corrosion properties of Ni−Si_3N_4 nanocomposite coatings. Bull Mater Sci 2014;37:721–8.
[2] Gomes A, Frade T, Nogueira ID. Morphological characterization of Zn-based nanostructured thin films. Current Microsc Contrib Adv Sci Technol 2012;2:1146.
[3] Fayomi OSI, Abdulwahab M, Popoola API. Properties evaluation of ternary surfactant-induced Zn-Ni-Al_2O_3 films on mild steel by electrolytic chemical deposition. J Ovonic Res 2013;9:123–32.
[4] Aal AA, Barakat MA, Mohamed RM. Electrophoreted Zn−TiO2−ZnO nanocomposite coating films for photocatalytic degradation of 2-chlorophenol. Appl Surf Sci 2008;254:4577–83.
[5] Su YL, Kao WH. Tribological behaviour and wear mechanism of MoS_2−Cr coatings sliding against various counterbody. Tribol Int 2003;36:11–23.
[6] Dong D, Chen XH, Xiao WT, Yang GB, Zhang PY. Preparation and properties of electroless Ni−P−SiO2 composite coatings. Appl Surf Sci 2009;255:7051–5.
[7] Popoola API, Fayomi OSI, Popoola MO. Electrochemical and mechanical properties of mild steel electro-plated with Zn-Al. Int J Electrochem Sci 2012;7:4898–917.
[8] Popoola API, Fayomi OSI. Effect of some process variables on zinc coated low carbon steel substrates. Sci Res Essays 2011;6(20):4264–72.
[9] Xia F, Tian J, Ma C, Potts M, Guo X. Effect of pulse frequency on microstructural, nanomechanical, and wear properties of electrodeposited Ni−TiN composite coatings. J Appl Phys 2014;116:234302.
[10] Ma C, Wu F, Ning Y, Xia F, Liu Y. Effect of heat treatment on structures and corrosion characteristics of electroless Ni−P−SiC nanocomposite coatings. Ceram Int 2014;40:9279–84.
[11] Xia F, Liu C, Ma C, Chu D, Miao L. Preparation and corrosion behavior of electrodeposited Ni−TiN composite coatings. Int J Refract Metals Hard Mater 2012;35:295–9.
[12] Zhu XB, Cai C, Zheng GQ, Zhang Z, Li JF. Electrodeposition and corrosion behavior of nanostructured Ni-TiN composite films. Trans Nonferrous Metals Soc China 2011;21:2216–24.
[13] Kumar KA, Mohan P, Kalaignan GP, Muralidharan VS. Electrodeposition and characterization of Ni-ZrO_2 nanocomposites by direct and pulse current methods. J Nanosci Nanotechnol 2012;12:8364–71.
[14] Cygan T, Wozniak J, Kostecki M, Adamczyk-Cieslak B, Olszyna A. Influence of graphene addition and sintering temperature on physical properties of Si_3N_4 matrix composites. Int J Refract Metals Hard Mater 2016;57:19–23.
[15] Malatji N, Popoola AP, Fayomi OS, Loto CA. Multifaceted incorporation of Zn-$Al_2O_3/Cr_2O_3/SiO_2$ nanocomposite coatings: anti-corrosion, tribological, and thermal stability. Int J Adv Manuf Technol 2016;82(5–8):1335–41.
[16] Sedmale G, Steins I, Zalite I, Mezinskis G. Microstructure and properties of mullite−ZrO_2 ceramics with silicon nitride additive prepared by spark plasma sintering. Ceram Int 2016;42:3745–50.
[17] Maros M, Németh AK, Károly Z, Bódis E, Maros Z, Tapasztó O, Balázsi K. Tribological characterisation of silicon nitride/multilayer graphene nanocomposites produced by HIP and SPS technology. Tribol Int 2016;93:269–81.
[18] Yu JJ, Guo WM, Zeng LY, Lin HT. Effect of SiO_2 addition on Si3N4 ceramics prepared by rapid nitridation and post-sintering route. Ceram Int 2017;43:13901–6.
[19] Logesh G, Lodhe M, Balasubramanian M. Effect of temperature and gaseous medium on the evolved microstructures of carbon fiber reinforced reaction bonded silicon nitride composites. Ceram Int 2017;43:6110–6.
[20] Surender M, Basu B, Balasubramaniam R. Wear characterization of electrodeposited Ni−WC composite coatings. Tribol Int 2004;37:743–9.
[21] Lu HH, Huang JL. Effect of Y_2O_3 and Yb_2O_3 on the microstructure and mechanical properties of silicon nitride. Ceram Int 2001;27(6):621–8.
[22] Lee CH, Lu HH, Wang CA, Nayak PK, Huang JL. Effect of heating rate on spark plasma sintering of a nanosized β-Si_3N_4-based powder. J Am Ceram Soc 2011;4(4):1182–90.
[23] Yang Y, Li B, Zhang C, Wang S, Liu K, Yang B. Fabrication and properties of graphene reinforced silicon nitride composite materials. Mater Sci Eng 2015;644:90–5.
[24] Bocanegra-Bernal MH, Matovic B. Mechanical properties of silicon nitride-based ceramics and its use in structural applications at high temperatures. Mater Sci Eng 2010;527(6):1314–38.
[25] Liu CC, Huang JL. Tribological characteristics of Si_3N_4-based composites in unlubricated sliding against steel ball. Mater Sci Eng 2004;384(1–2):299–307.
[26] Greskovich C, Prochazka S. Stability of Si3N4 and liquid phase (s) during sintering. J Am Ceram Soc 1981;64(7):C96–7.
[27] Riley FL. Silicon nitride and related materials. J Am Ceram Soc 2000;83(2):245–65.
[28] Zou C, Zhang C, Li B, Wang S, Cao F. Microstructure and properties of porous silicon nitride ceramics prepared by gel-casting and gas pressure sintering. Mater Des 2013;44:114–8.
[29] Anawe PA, Raji O, Fayomi OS. Evaluation of responses from electrolytic multilayer hybrid coating for extended application. Procedia Manuf 2017;7:562–6.
[30] Shibli SM, Chacko F, Divya C. Al_2O_3−ZrO_2 mixed oxide composite incorporated aluminium rich zinc coatings for high wear resistance. Corrosion Sci 2010;52:518–25.
[31] Daniyan AA, Umoru LE, Fayomi OS. Structural evolution, optoelectrical and corrosion properties of electrodeposited WO_3 integration on Zn-TiO_2 electrolyte for defence super application. Defence Technol 2018:1–7.
[32] Low CT, Wills RG, Walsh FC. Electrodeposition of composite coatings containing nanoparticles in a metal deposit. Surf Coating Technol 2006;12(1–2):371–83. 201.
[33] Achi SS. Basic principles of coating technology. Shemang Graphics; 2003. p. 1–2. Zaria Nigeria.
[34] Fayomi OSI, Abdulwahab M. Property's evaluation of ternary surfactant-induced Zn-Ni-Al_2O_3 films on mild steel by electrolytic chemical deposition. J Ovonic Res 2013;5:123–32.
[35] Fayomi OSI, Akande IG, Popoola API. Corrosion protection effect of chitosan on the performance characteristics of A6063 alloy. J Bio Tribo Corrosion 2018;4:73.
[36] Hosking NC, Ström MA, Shipway PH, Rudd CD. Corrosion resistance of zinc−magnesium coated steel. Corrosion Sci 2007;49(9):3669–95.
[37] Boshkov N. Galvanic Zn−Mn alloys—electrodeposition, phase composition, corrosion behaviour and protective ability. Surf Coating Technol

Please cite this article as: Akande IG et al., Optimizing the defensive characteristics of mild steel via the electrodeposition of Zn−Si_3N_4 reinforcing particles, Defence Technology, https://doi.org/10.1016/j.dt.2018.11.001

2003;172(2–3):217–26.
[38] Mouanga M, Berçot P, Rauch JY. Comparison of corrosion behaviour of zinc in NaCl and in NaOH solutions. Part I: corrosion layer characterization. Corrosion Sci 2010;52(12):3984–92.
[39] Mouanga M, Ricq L, Douglade J, Berçot P. Corrosion behaviour of zinc deposits obtained under pulse current electrodeposition: effects of coumarin as additive. Corrosion Sci 2009;51(3):690–8.
[40] Qu Q, Li L, Bai W, Yan C, Cao CN. Effects of NaCl and NH4Cl on the initial atmospheric corrosion of zinc. Corrosion Sci 2005;47(11):2832–40.
[41] Boshkov N, Petrov K, Vitkova S, Nemska S, Raichevsky G. Composition of the corrosion products of galvanic alloys Zn–Co and their influence on the protective ability. Surf Coating Technol 2002;157(2–3):171–8.
[42] El Wanees SA, Radwan AB, Alsharif MA, El Haleem SA. Initiation and inhibition of pitting corrosion on reinforcing steel under natural corrosion conditions. Mater Chem Phys 2017;190:79–95.
[43] Xiang Y, Li C, Hesitao W, Long Z, Yan W. Understanding the pitting corrosion mechanism of pipeline steel in an impure supercritical CO_2 environment. J Supercrit Fluids 2018;138:132–42.
[44] Anawe PA, Raji O, Fayomi OS, Efeovbohkan VE. Influence of composite nano coating on ternary sulphate Co-deposition: corrosion and surface characterization. Procedia Manuf 2017;7:556–61.
[45] Wang TG, Jeong D, Liu Y, Wang Q, Iyengar S, Melin S, Kim KH. Study on nanocrystalline Cr_2O_3 films deposited by arc ion plating: II. Mechanical and tribological properties. Surf Coating Technol 2012;206(10):2638–44.
[46] Fayomi OSI, Atayero AA, Mubiaye P, Akande IG, Adewuyi PA, Fajobi MA, Ayara WA. Mechanical and opto-electrical response of embedded smart composite coating produced via electrodeposition technique for embedded system in defence application. J Alloy Comp 2019;773:305–13.
[47] Dutta A, Saha SK, Adhikari U, Banerjee P, Sukul D. Effect of substitution on corrosion inhibition properties of 2-(substituted phenyl) benzimidazole derivatives on mild steel in 1 M HCl solution: a combined experimental and theoretical approach. Corrosion Sci 2017;123:256–66.
[48] Rossrucker L, Samaniego A, Grote JP, Mingers AM, Laska CA, Birbilis N, Frankel GS, Mayrhofer KJ. The pH dependence of magnesium dissolution and hydrogen evolution during anodic polarization. J Electrochem Soc 2015;7:333–9.
[49] Frankel GS. Fundamentals of corrosion kinetics. In: Active protective coatings. Dordrecht: Springer; 2016. p. 17–32.
[50] Fayomi OSI, Akande IG, Oluwole OO, Daramola D. Effect of water soluble chitosan on the electrochemical corrosion behaviour of mild steel. Chem Data Collect 2018;17–18:321–6.
[51] Khorsand S, Raeissi K, Ashrafizadeh F. Corrosion resistance and long-term durability of super-hydrophobic nickel film prepared by electrodeposition process. Appl Surf Sci 2014;305:498–505.
[52] Popoola API, Daniyan AA, Umoru LE, Fayomi OSI. Effect of WO_3 nanoparticles loading on the microstructural, mechanical and corrosion resistance of Zn matrix/TiO_2-WO_3 nanocomposite coatings for marine application. J Mar Sci Appl 2017;16. 1389-1387.
[53] Benabid S, Douadi T, Issaadi S, Penverne C, Chafaa S. Electrochemical and DFT studies of a new synthesized Schiff base as corrosion inhibitor in 1 M HCl. Measurement 2017;99:53–63.
[54] Gupta RK, Malviya M, Verma C, Quraishi MA. Aminoazobenzene and diaminoazobenzene functionalized graphene oxides as novel class of corrosion inhibitors for mild steel: experimental and DFT studies. Mater Chem Phys 2017;198:360–73.
[55] Haque J, Verma C, Srivastava V, Quraishi MA, Ebenso EE. Experimental and quantum chemical studies of functionalized tetrahydropyridines as corrosion inhibitors for mild steel in 1 M hydrochloric acid. Results Phys 2018;9:1481–93.
[56] Zakaria K, Negm NA, Khamis EA, Badr EA. Electrochemical and quantum chemical studies on carbon steel corrosion protection in 1 M H_2SO_4 using new eco-friendly Schiff base metal complexes. J Taiwan Inst Chem Eng 2016;61:316–26.
[57] Dohare P, Chauhan DS, Hammouti B, Quraishi MA. Experimental and DFT investigation on the corrosion inhibition behavior of expired drug lumerax on mild steel in hydrochloric acid. Anal Bioanal Electrochem 2017;9:762.
[58] Anejjar A, El Mouden OI, Batah A, Bouskri A, Rjoub A. Corrosion inhibition potential of ascorbic acid on carbon steel in acid media. Appl J Environ Eng Sci.;3:3-1.
[59] Yang SF, Wen Y, Yi P, Xiao K, Dong CF. Effects of chitosan inhibitor on the electrochemical corrosion behavior of 2205 duplex stainless steel. Int J Miner Metall, Mater 2017;24:1260–6.
[60] Soares H, Zucarelli T, Vieira M, Freitas M, Reis L. Experimental characterization of the mechanical properties of railway wheels manufactured using class B material. Procedia Struct Integr 2016;1:265–72.
[61] Wang X, Chan HL, Choy CL. Piezoelectric and dielectric properties of CeO_2-added (Bi0. 5Na0. 5) 0.94 Ba0. 06TiO_3 lead-free ceramics. Solid State Commun 2003;8:395–9.
[62] Subasri R, Shinohara T, Mori K. Modified TiO_2 coatings for cathodic protection applications. Sci Technol Adv Mater 2005;5:501.
[63] Rusu DE, Ispas A, Bund A, Gheorghies C, Carac G. Corrosion tests of nickel coatings prepared from a Watts-type bath. J Coating Technol Res 2012;1:87–95.

Please cite this article as: Akande IG et al., Optimizing the defensive characteristics of mild steel via the electrodeposition of Zn–Si_3N_4 reinforcing particles, Defence Technology, https://doi.org/10.1016/j.dt.2018.11.001